Available online at www.sciencedirect.com
ScienceDirect
Scripta Materialia 59 (2008) 440–443
Scripta MATERIALIA
www.elsevier.com/locate/scriptamat

Growth directions in directionally solidified Al–Zn and Zn–Al alloys near eutectic composition

M. Rhême, F. Gonzales* and M. Rappaz

Computational Materials Laboratory, Ecole Polytechnique Fédérale de Lausanne, Station 12, Lausanne CH-1015, Switzerland

Received 14 March 2008; revised 11 April 2008; accepted 14 April 2008
Available online 24 April 2008

Growth directions and crystallographic orientations of solidification microstructures have been measured in Al–Zn alloy near the eutectic composition. Al dendrites in Al–92 wt.% Zn alloy were found to grow along the $\langle 1\,1\,0\rangle$ directions while Zn dendrites in Al–96 and 98 wt.% Zn have $\langle 1\,0\,\bar{1}\,0\rangle$ trunks. In the lamellar eutectic, a crystallographic relationship has been found between the dense plane of each phase, i.e. $\{1\,1\,1\}_{fcc}\|\{0\,0\,0\,1\}_{hcp}$, and the dense directions, i.e. $\langle 1\,1\,0\rangle_{fcc}\|\langle 1\,\bar{2}\,1\,0\rangle_{hcp}$.

Keywords: Al–Zn; Directional solidification; Dendritic growth; Eutectic solidification; Growth directions

Aluminum–zinc alloys constitute an important class of wrought alloys, the so-called 7000 series, and are also widely used as anti-corrosion coatings of steel sheets. They are also interesting from a more fundamental point of view because zinc, a hexagonal close-packed (hcp) element, can be added to aluminum up to very large amounts (up to 94 wt.%) while keeping the face-centered cubic (fcc) structure. During solidification of hypoeutectic alloys, fcc dendrites form despite large amounts of zinc in solid solution at high temperature, while hcp ones normally grow for hypereutectic compositions. However, an interesting phenomenon has been reported recently [1] concerning the growth direction of fcc dendrites: while $\langle 100\rangle$ dendrites are normally expected to grow in cubic metals [2], a continuous transition from $\langle 1\,0\,0\rangle$ to $\langle 1\,1\,0\rangle$ has been observed as the concentration of zinc c_{Zn} increases from 5 to 90 wt.%. This evolution, called dendrite orientation transition (DOT), occurred between 25 and 60 wt.%. Textured seaweed structures were observed at the beginning and end of this DOT.

This change of dendrite orientation in fcc Al–Zn was interpreted as a modification of the solid–liquid interfacial energy of aluminum $\gamma_{s\ell}(c_{Zn})$ as c_{Zn} increases [1,3]. Indeed, dendrite growth directions are dictated by the anisotropy of $\gamma_{s\ell}$; more precisely they are given by minima of the so-called interface stiffness $S_{s\ell}$. The stiffness $S_{s\ell}$ is given in two dimensions by $(\gamma_{s\ell} + \gamma''_{s\ell})$, where $\gamma''_{s\ell}$ is the second angular derivative of $\gamma_{s\ell}(\phi)$ appearing in Herring's relations [4]. The stiffness in three dimensions is similarly given by $\gamma_{s\ell} + \nabla^2\gamma_{s\ell}$, where the Laplacian is applied to $\gamma_{s\ell}(\theta, \phi)$. In two dimensions, the minima of the stiffness correspond to the most convex parts of the equilibrium shape crystal, from which dendrites will be initiated naturally, and such is also normally the case in three dimensions. Note that the equilibrium shape crystal can be obtained from the γ-plot and vice versa using the ξ-vector construction outlined by Cahn and Hofmann [5]. In the case of aluminum, the anisotropy of $\gamma_{s\ell}$ has been measured in Al–Cu with a low copper composition [6] and is very low, typically 1%. On the other hand, it is much higher in hcp zinc (about 30% between the c-direction and the basal plane) [7] and causes dendrites to grow primarily along the $\langle 1\,0\,\bar{1}\,0\rangle$ directions. $\langle 0\,0\,0\,1\rangle$ dendrites can also grow in Zn–Al, but with a velocity about half that of $\langle 1\,0\,\bar{1}\,0\rangle$ dendrites [11].

Since zinc influences the growth of aluminum dendrites, the question that is addressed in the present report is the following: is it possible to influence the growth directions of zinc dendrites by aluminum solute elements and make them grow along $\langle 1\,1\,\bar{2}\,0\rangle$, i.e. the equivalent of $\langle 1\,1\,0\rangle$ in fcc, instead of $\langle 1\,0\,\bar{1}\,0\rangle$ direction? The question might look absurd considering the large anisotropy of $\gamma_{s\ell}$ for zinc, however, one should keep in mind that the 30% anisotropy mentioned before is only between the c-axis and the basal plane. The anisotropy in the basal plane has not been measured to the authors' knowledge.

Therefore, in the present work, three different alloy compositions were prepared from Al 99.995% and Zn

* Corresponding author. Tel.: +41 788357177; e-mail: frederic.gonzales@epfl.ch

1359-6462/$ - see front matter © 2008 Acta Materialia Inc. Published by Elsevier Ltd. All rights reserved.
doi:10.1016/j.scriptamat.2008.04.017

99.995%: one hypoeutectic (Al–92 wt.% Zn) and two hypereutectic (Al–96 and 98 wt.% Zn). These compositions are indicated by dashed lines on the Al–Zn phase diagram reproduced in Figure 1A. The right amounts of each metal were melted, mixed together and cast in a horizontal copper mold to prevent macrosegregation. Rods 200 mm long and 4.9 mm in diameter were then machined from the ingots. They were then inserted into alumina crucibles for directional solidification in the same Bridgman furnace used in Ref. [1]. While the thermal gradient was about the same (about 40 °C cm^{-1}), the pulling speed was reduced by a factor 10 as compared with that used in Ref. [1] (i.e. 6.7 μm s^{-1} was selected in the present case). Indeed, as pointed out by Sémoroz et al. [11], too large a velocity in the hypereutectic alloys induces the formation of equiaxed grains, unless poisoning solute elements such as Pb, Bi or Sb are added.

For metallographic observations, transverse and longitudinal sections were made using a diamond saw. The sections were then mechanically polished according to the following sequence: 1000–2400 SiC paper and water as lubricant, polishing cloth with 6, 1 and 1/4 μm diamond particles with ethanol as lubricant. Etching was then performed with 25% Keller solution, a short dipping of about 1 s being sufficient to reveal the microstructure. The same procedure was applied for electron backscatter diffraction (EBSD) analyzes. No etching or treatment was needed for the hypereutectic composition. For the hypoeutectic composition, electropolishing was performed at a temperature of about 10–20 °C, for 8 s, with 10 V and a solution made of 72 ml ethanol, 20 ml 2-butoxyethanol and 8 ml perchloric acid (71% concentration). The EBSD observations were performed on a Philips XL30FEG scanning electron microscope (typically 25 kV, spot size of a few nm, working distance between 20 and 25 mm). The recording and indexing of the pseudo-Kikuchi lines were performed with the software Channel 5 from HKL Technology. EBSD maps were made of longitudinal and transverse sections, in the primary trunk of the columnar dendrites. The crystallographic relationship between the fcc and hcp phases in the interdendritic eutectic was also identified using EBSD maps on transverse sections.

Starting first with the interdendritic eutectic, Figure 1B shows two eutectic grains, each one made of Al (dark) and Zn (light) lamellae. The lamellae interspacing in this regular eutectic is 2.4 ± 0.5 μm. A lever rule applied on the phase diagram gives an Al volume fraction of 0.21, while metallographic observations give a value of about 0.12. In fact, the monotectoid transformation also occurs in the Al lamellae, partially transforming this phase into Zn and lower solute-content fcc. Singh et al. [8] showed that the excess Zn that precipitates represents 15% of the total volume of Zn, of which about half precipitates at the interface of the lamellae and the other half at the center of the Al lamellae.

Pole figures obtained for the fcc and hcp lamellae of the two grains are also shown in Figure 1B. As can be seen, there is a clear orientation relationship between these two phases in the two grains:

$$\langle 1\bar{2}10\rangle_{hcp} \| \langle 110\rangle_{fcc}$$
$$\{0001\}_{hcp} \| \{111\}_{fcc}$$

This crystallography relationship, which corresponds to the dense directions and dense planes in both the hcp and fcc phases, comes from the initial stage of nucleation of the second phase over the first one. On the other hand, the interfaces between Zn and Al lamellae do not correspond exactly to the dense packing planes as can be seen on the micrograph: they are within about 10° from the basal or (1 1 1) plane, i.e. incoherent interfaces. During growth, this regular eutectic has some freedom to adapt the interfaces as a function of the thermal conditions while keeping the original crystallographic relationship. These metallographic observations confirm studies made by previous authors [9,8,10].

Longitudinal sections of the two hypereutectic alloys are shown in Figure 1C and D together with corresponding $\langle 10\bar{1}0\rangle$ pole figure. The axes of the metallographic sections and pole figures are the same, i.e. the normal to the section is at the center of the pole figure. As can be seen, both sections are within 10° of the basal plane. More importantly, the dendrite growth direction in both specimens correspond to $\langle 10\bar{1}0\rangle$ as indicated by the point near the label X_0 in the pole figure. This growth direction is identical to that measured by Sémoroz et al. [11] in zinc alloys with various aluminum concentrations and by Quiroga et al. [13] in Zn–0.2 wt.%Al. This seems to confirm that aluminum does not change the regular $\langle 10\bar{1}0\rangle$ growth direction of Zn dendrites in the basal plane. The dendrite side arms in the Al–96 wt.% Zn specimen (Fig. 1C) are fairly well-developed along $\langle 10\bar{1}0\rangle$, i.e. at 60° from the trunks, whereas the dendrites in the Al–98 wt.% Zn specimen look more cellular (Fig. 1D). This effect is probably due to the influence of the solidification interval $\Delta T_0(c_{Zn})$ rather than induced by a change of the strength of the anisotropy of $\gamma_{s\ell}$ in the basal plane (i.e. the contribution of the spherical harmonics $\epsilon_6^6(Y_6^6 + Y_6^{-6})$ in the development of $\gamma_{s\ell}$). Indeed, in the Al–98 wt.% Zn specimen, the solidification interval is 50 K and the limit of constitutional undercooling $v_c = GD_\ell/\Delta T_0$, where D_ℓ is the coefficient in the liquid, is around 0.25 μm s^{-1}. This value is closer to the 0.67 μm s^{-1} used in the present experiments and so the microstructure is more cellular. Nevertheless, they are not strictly speaking cells since the primary trunks grow along a preferential direction. In order to assess more quantitatively the strength of the term ϵ_6^6, direct measurements of the equilibrium shape of zinc droplets in the solid are underway.

A cross-section of the Al–98 wt.% Zn specimen is shown in Figure 2. The dendrites look really elongated in the basal plane with not very well-developed side arms. The dendrite trunk spacing, as measured in a transverse section, is fairly anisotropic due to the different growth rates of $\langle 10\bar{1}0\rangle$ and $\langle 0001\rangle$ side arms. It is about 260 μm along the basal plane while only 100 μm separate two successive rows of dendrites along the *c*-direction. In the corresponding pole figure shown in Figure 2, two orientations are measured locally at a given spot of the electron beam, which is rather surprising. The circular dots correspond to the orientation measured in the longitudinal section (Fig. 1), i.e. the $\langle 10\bar{1}0\rangle$ of the dendrite trunk corresponds to the normal to the transverse section or to the thermal gradient direction. The *c*-axis of the square dots shown in this

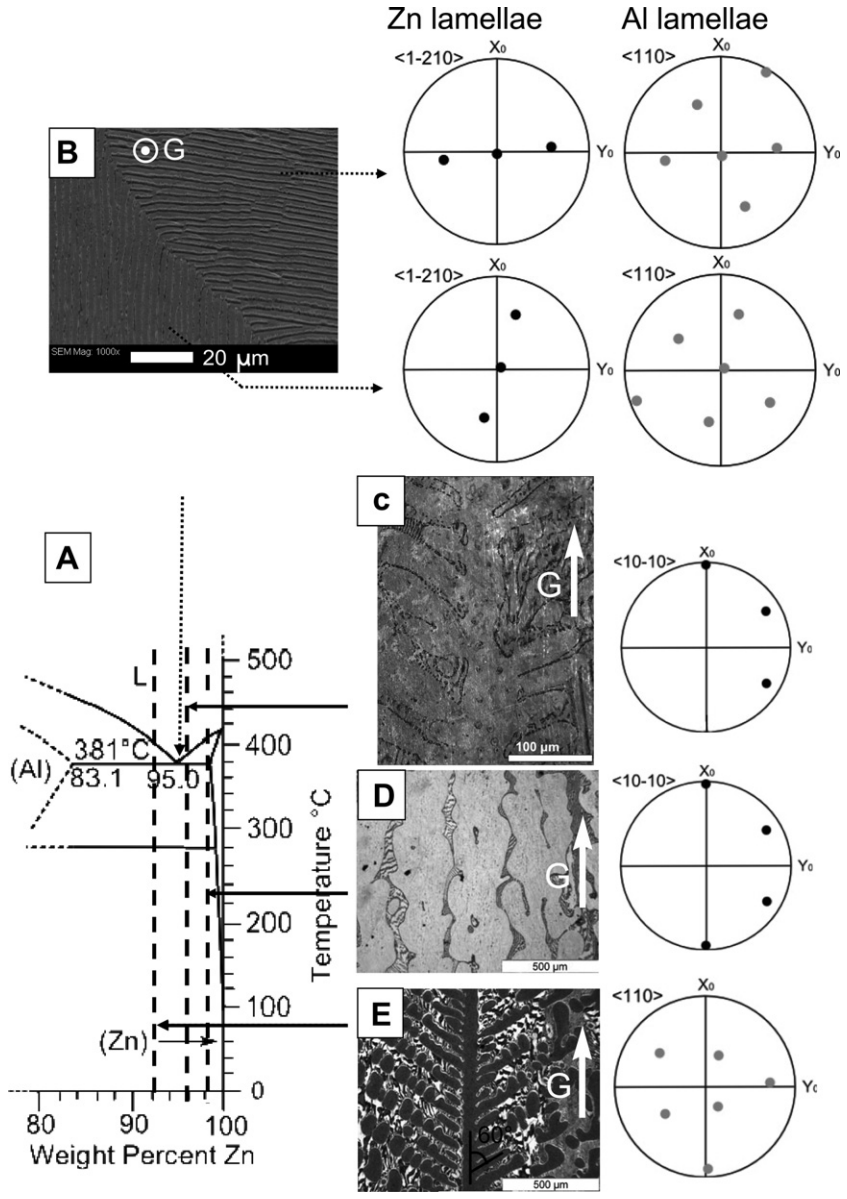

Figure 1. (A) Zn-rich side of the Al–Zn phase diagram redrawn from Ref. [12]. Dashed lines show the three studied compositions shown in (C)–(E). (B) Transverse SEM picture of two grains of the eutectic region. The associated pole figures are shown on the right for each phase (fcc and hcp) in the two different grains. Longitudinal section micrographs observed in (C) Al–96 wt.% Zn sample (SEM), (D) Al–98 wt.% Zn sample (OM) and (E) Al–92 wt.% Zn sample. For figures (C) and (D), the $\langle 10\bar{1}0\rangle$ pole figures correspond to the hcp Zn dendrites, while for figure (E), the $\langle 110\rangle$ pole figure is for the fcc Al dendrites. Growth rate 0.67 μm s^{-1}; thermal gradient 40 K cm^{-1}.

figure is at 90° from this orientation and probably corresponds to microtwinned domains induced by the sample preparation.

In the hypoeutectic sample, Al dendrites undergo a monotectoid transformation $\alpha \rightarrow \alpha' + \beta$. Transmission electron microscopy (TEM) observations showed that this solid state transformation causes a crystallographic rearrangement under the form of a lamellar structure. The interlamellar spacing is variable, depending of the part observed, but is generally less than 1 μm. As a result, the EBSD signal is very poor but a few points could nevertheless be indexed. As shown in Figure 1E, Al dendrites of the hypoeutectic alloy grow along $\langle 110\rangle$ (grey point at the bottom), as already found for Al–90 wt.% Zn [1]. This result is confirmed by the metallographic observations shown in this figure: although side arms

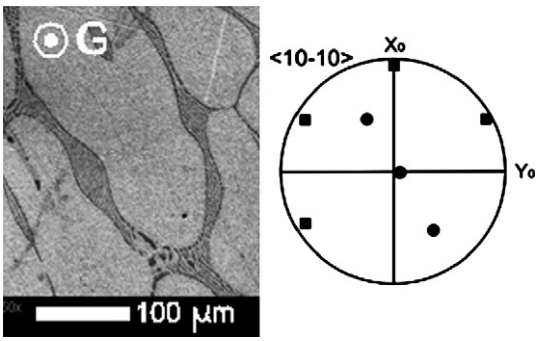

Figure 2. SEM picture of a transverse section of the hypereutectic Al–98 wt.%Zn alloy showing a zinc dendrite trunk and associated $\langle 10\bar{1}0\rangle$ pole figure measured in its center and showing two sets of directions (dots and squares).

are not in this plane of the micrograph, as shown by their fragmented aspect, they make an angle of about 60° with the trunk.

In conclusion, in the fcc structure, the minima of the solid–liquid interface stiffness do correspond to the nearest-neighbor directions, i.e. $\langle 1\,1\,0\rangle$ direction, while they are at 30° from these directions in the hcp structure, i.e. $\langle 1\,0\,\bar{1}\,0\rangle$, regardless of the Al composition.

[1] F. Gonzales, M. Rappaz, Met. Mat. Trans. 37A (2006) 2797.
[2] Fundamentals of Solidification, Trans Tech, Switzerland, 1989.
[3] T. Haxhimali, A. Karma, F. Gonzales, M. Rappaz, Nature Mater. 5 (2006) 660.
[4] C. Herring, Phys. Rev. 82 (1951) 87.
[5] D.W. Hoffman, J.W. Cahn, Surf. Sci. 31 (1972) 368.
[6] S. Liu, R.E. NapolitanoR. Trivedi, Acta Mater. 49 (2001) 4271.
[7] A. Passerone, N. Eustathopoulos, Acta Mater. 30 (1982) 1349.
[8] B. Singh, I.O. Smith, G.A. Chadwick, J. Cryst. Growth 37 (1977) 301–308.
[9] D.D. Double, P. Truelove, A. Hellawell, J. Cryst. Growth 2 (1968) 191–198.
[10] K. Ito, K. Fujimoto, J. Cryst. Growth 48 (1980) 141–148.
[11] A. Sémoroz, L. Strezov, M. Rappaz, in: M. Lamberights (Ed.), Galvatech 2001, Verlag Stahleisen, 2001, p. 612.
[12] T.B. Massalski (Ed.), Binary Alloy Phase Diagrams, ASM International, Materials Park, OH, 1986.
[13] A. Quiroga, S. Claessens, B. Gay, M. Rappaz, Met. Mater. Trans. 35A (2004) 3543.